# PASSDOP BASED ON FIRING STABLE A-SINX:P AS A CONCEPT FOR THE INDUSTRIAL IMPLEMENTATION OF N-TYPE PERL SILICON SOLAR CELLS

Bernd Steinhauser, Muhammad bin Mansoor, Ulrich Jäger, Jan Benick, Martin Hermle
Fraunhofer Institute for Solar Energy Systems, Heidenhofstrasse 2, D-79110 Freiburg
Ph +49 761 4588 5190, Fax +49 761 4588 9250
Email: bernd.steinhauser@ise.fraunhofer.de

ABSTRACT: In this work, we present an approach to create a PERL structure for n-type silicon solar cells which is compatible with the high temperature step applied for firing of screen printed contacts. This approach is based on the *PassDop* concept presented by Suwito *et. al.* The *PassDop* approach combines a doped passivation layer with a laser process to create a local back surface field on the rear side. As the original *PassDop* layer—based on a-$SiC_x$:P—is not firing stable, we developed a new layer based on phosphorous doped a-$SiN_x$, the *fPassDop* layer. This layer provides a good passivation with an effective recombination velocity <5 cm/s after a firing step. For the local back surface field, a sheet resistance in the range of 60 Ω/sq was measured after applying the laser process. In a first batch, we applied this layer to small area solar cells achieving a conversion efficiency of 21.3 % (675 mV) with evaporated front contacts. As a proof of concept, we applied this layer to large area n-type solar cells with screen printed front side contacts achieving an efficiency of 20.1 % with a $V_{oc}$ of 668 mV.
Keywords: n-type, Passivation, Laser Processing, Silicon-Nitride

## 1 INTRODUCTION

*n*-type passivated emitter and rear locally diffused (PERL) silicon solar cells have proven to offer a high efficiency potential [1]. The *PassDop* approach introduced by Suwito *et al.* demonstrated an industrially feasible realization of such a structure (Figure 1, [2]), based on a-$SiC_x$:P. Unfortunately this layer stack showed strong degradation after a high temperature step, which is necessary for the firing of screen printed contacts (see Figure 2). For an industrially feasible *PassDop* process, it is therefore necessary to develop an alternative solution which is compatible with the screen printing technique.

Amorphous silicon nitride is the state of the art technology for the passivation of phosphorous emitters and is known to provide good passivation after a firing step on both p-type and n-type base material respectively [3-5]. While the formation of an inversion layer results in parasitic shunting on p-type silicon solar cells [6], a-$SiN_x$ is suitable for n-type rear side passivation due to the formation of an accumulation layer. Silicon nitride can be doped by both phosphorous and boron, and thus has already been used to form selective emitters [7-9].

Our approach combines all of these techniques to provide a firing-stable *PassDop* (*fPassDop*) layer stack based on amorphous, phosphorous doped silicon nitride. It can be used to passivate the surface and form a local back surface field (LBSF) by applying a suitable laser process and hence to fabricate n-type PERL silicon solar cells with fired screen-printed front side contacts.

## 2 EXPERIMENTAL

### 2.1 The *PassDop* Process

The *PassDop* process sequence (see Figure 1) is a simple way to process the rear side of an n-type PERL silicon solar cell. In a first step the doped dielectric layer is deposited. This wafer has to provide a sufficient level of surface passivation as well an appropriate amount of dopants. After the deposition (e.g. by plasma-enhanced chemical vapor deposition (PECVD)), the layer is opened in a laser process. During the laser pulse, the silicon is molten and the dopants are driven into the silicon. After solidification the doped silicon forms a local back surface field (LBSF). This LBSF is contacted by applying a metal to the rear side, usually by evaporation of aluminum. For the integration into the solar cell process with screen printed contacts, it is necessary to introduce the firing step after deposition of the layer and before evaporation of the rear side metal.

In this paper, three different *PassDop* layers based on doped a-$SiN_x$ were investigated, i) a single layer system, ii) a double layer system "Gen 1" and iii) an advanced double layer system "Gen 2". A single layer represents the simplest possible system to create a *PassDop* layer. In the double layer system surface passivation and doping are decoupled. These enhanced stacks are denoted as *fPassDop*.

For the deposition of the layers, an AK800 PECVD reactor by Roth & Rau was used. This reactor uses microwave plasma excitation similarly to common inline PECVD reactors. Therefore, a process transfer to larger machines is feasible, even though the AK800 is a laboratory batch type reactor. We used silane, argon, molecular nitrogen and diluted phosphine as precursor gases to deposit the a-$SiN_x$:P layers.

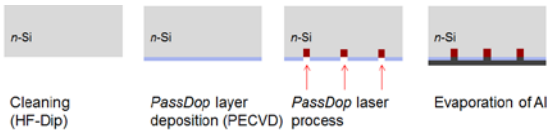


**Figure 1**: *PassDop* process sequence: 1. Cleaning of the wafer 2. Deposition of the *PassDop* layer 3. Local opening of the *PassDop* layer and simultaneous diffusion of the dopant into the silicon to form a LBSF 4. Evaporation of aluminum to create a contact. For a *PassDop* cell with screen printed contacts, the firing step has to be introduced after step 2 and before step 4.

### 2.2 Sample Preparation

We used n-type 1 Ωcm float-zone silicon wafers for the characterization of the passivation properties. These samples were symmetrically coated with the *fPassDop* layer as depicted in Figure 3 (left). Prior to the deposition, the samples were cleaned in $HNO_3$ and HF. After the passivation, the samples were fired in a single

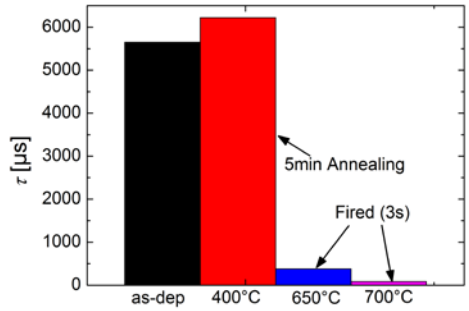


**Figure 2**: Effective lifetime of a-SiC$_x$ passivated silicon wafers after different post deposition high temperature processes.

wafer rapid thermal processing reactor calibrated for this sample structure. The peak temperature was applied for 3 s. To extract the effective minority carrier lifetime, we used a WCT-120 quasi-steady state photoconductance measurement tool by Sinton Consulting. The effective surface recombination velocity was calculated from the measured lifetime [10] by applying the Auger model of Kerr *et. al.* to account for the bulk lifetime [11].

To measure the doping profile and the corresponding sheet resistance, we deposited the *fPassDop* layers on p-type 10 Ωcm float-zone silicon wafers. These samples were processed with a Jenoptic IR70 (30 kHz, $\lambda$ = 1030 nm, [12]) to create overlapping point structures, which resulted in measurable 20×20 mm² doped areas (see Figure 3 (right)). The sheet resistance was measured by applying the four-point probe technique. The doping profiles were determined with a WEP CPV21 wafer profiler by electrochemical capacity voltage (ECV) profiling.

### 2.3 Solar Cells

Two types of n-type PERL silicon solar cells were processed on $\rho$ = 1 Ωcm n-type float-zone material, i) small area (20×20 mm²) solar cells with PVD contacts on both sides and ii) large area (125×125 mm$^2$ pseudo square) solar cells with screen printed front contacts (see Figure 4)

The small area cells were processed with the single layer as well as the *fPassDop* Gen 1 process. The process sequence with the most important steps for these cells is shown in Figure 4 (a). To mask the rear side from texture formation and boron diffusion, a thermal oxidation was performed, followed by etch back of the silicon oxide on the front side. With this mask, texturization in KOH and tube furnace $BBr_3$ boron diffusion were performed in the active cell area to create a 90 Ω/sq emitter on inverted pyramids. This emitter was passivated by a stack of $Al_2O_3$ and $SiN_x$. After the front side passivation, the *PassDop* deposition and laser steps were done before firing the wafers at 810°C in an inline fast firing furnace. This "dummy" firing step without metallization was done

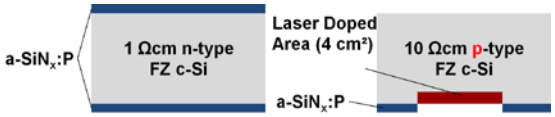


**Figure 3**: Left: Structure used to extract lifetime and SRV Right: Structure used to measure $R_{Sheet}$ and doping profile.

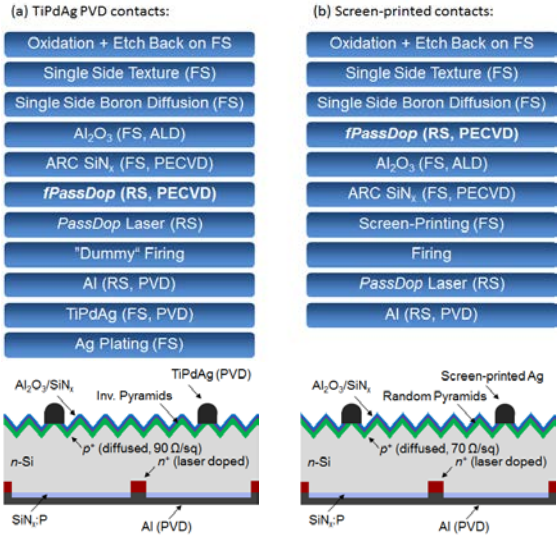


**Figure 4**: Sketch of the important steps in the process sequence and sketch of the cell structure used for solar cells with PVD (a) and screen printed (b) contacts.

to simulate the effect of the firing step necessary for the contact formation of screen printed pastes. Finally, the solar cells were metallized by evaporation of aluminum on the rear and a stack of titan, palladium and silver on the front side. The front side seed layer was thickened by silver plating.

For the large area solar cells (125×125 mm²) with screen printed contacts on the front side (see Figure 4 (b)) the improved *fPassDop* Gen 2 process was used. The process sequence with the most important steps for these cells is shown in Figure 4 (b). Similarly to the small area cells, we used thermal oxidation to mask the rear side. In contrast to the small area cells, texturization in KOH was performed to create random pyramids. Tube furnace $BBr_3$ boron diffusion was performed to create a 70 Ω/sq emitter. For these cells, the *PassDop* deposition was done prior to the front side passivation. After passivation, the front side contacts were printed in a single screen printing step followed by a firing step in an inline fast firing furnace at 770°C set temperature. After firing, the *PassDop* laser process was applied to the rear side followed by evaporation of aluminum in an inline high-throughput evaporation machine.

## 3 RESULTS AND DISCUSSION

The resulting lifetimes and corresponding surface recombination velocities $S_{eff}$ for the three different *PassDop* layers are shown in Figure 5. Both the single layer as well as *fPassDop* Gen 1 show a dependence of the measured lifetime on the firing temperature. Starting at 600-900 µs at a peak temperature of 700°C the determined lifetime increases to approx. 1.5 ms for a peak temperature of 850°C. For *fPassDop* Gen 2, no such dependency was found. For this layer we determined a lifetime of approx. 1.6 ms in the range of 700-850°C peak temperature. Therefore, we achieved a $S_{eff}$ less than 10 cm/s for the *fPassDop* layers in the selected peak temperature range, proving the firing stability of the developed *fPassDop* passivation. The behavior of Gen 2 is desirable, as it allows for the optimization of the firing

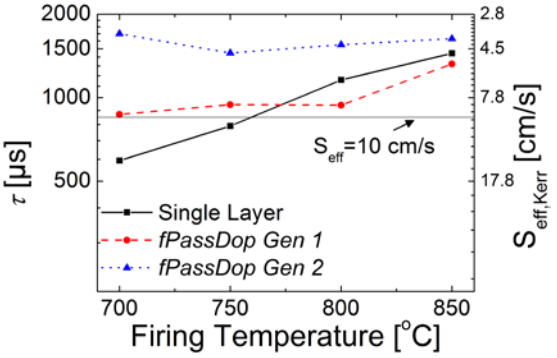


**Figure 5**: Effective lifetime and surface recombination velocity for the a-$SiN_x$:P based *PassDop* layers after firing: 1. single layer a-$SiN_x$:P 2. *fPassdop* layer (Gen 1) 3. improved *fPassDop* layer (Gen 2).

process to the necessities of the front side screen printing paste.

For these three layers, the determined sheet resistance is shown in Figure 6. For all layers, first the sheet resistance decreased with increasing laser power. For the single layer, a minimum sheet resistance of 100 Ω/sq was reached at a laser power around 9 to 10 Watts. In case of the *fPassDop* layers, higher laser powers around 13 W are needed to reach the sheet resistance minimum (a further increase in the laser power would result in an increase of the sheet resistance due to ablation). A minimum of around 80 Ω/sq for Gen 1 and around 60 Ω/sq for Gen 2 showed that the doping efficiency of the layer stack system can be strongly improved compared to the single layer. Examples for the measured phosphorous profiles for *fPassDop* Gen 1 are shown in Figure 7. At lower laser powers (~7 W), the resulting profile featured a very low surface concentration below

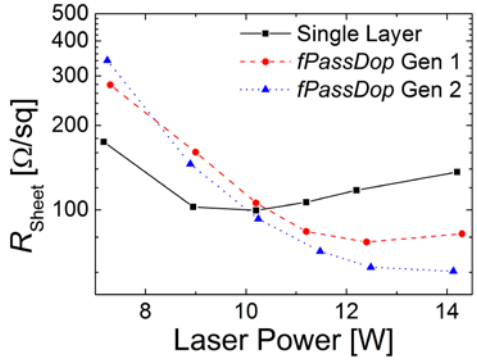


**Figure 6**: Resulting sheet resistance for the different a-$SiN_x$:P based *PassDop* layers after applying the laser process.

**Table I**: Measured cell parameters for the best cells of each type: a) Single layer b) *fPassDop* Gen 1 (both 4 $cm^2$ with PVD contacts) c) *fPassDop* Gen 2 with screen printed contacts (148.7 $cm^2$). Certified measurements by Fraunhofer ISE CalLab (except *PFF*).

| Cell | $V_{oc}$ [mV] | $J_{sc}$ [mA/cm²] | *FF* [%] | *PFF* [%] | $\eta$ [%] |
|---|---|---|---|---|---|
| a | 672 | 39.0 | 77.7 | 83.3 | 20.3 |
| b | 675 | 38.9 | 80.9 | 83.7 | 21.3 |
| c | 668 | 38.4 | 78.2 | 82.9 | 20.1 |

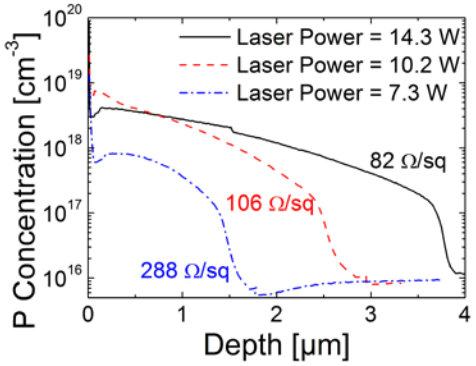


**Figure 7**: Doping profiles after applying the laser process with varying power to *fPassDop* Gen 1. Profiles were measured by the ECV technique.

$1\times10^{18}$ $cm^{-3}$ with a very high sheet resistance (288 Ω/sq). At ~10 W laser power, the resulting profile became deeper (~2.6 µm) with a sheet resistance of 106 Ω/sq, while the surface concentration increased to $9\times10^{18}$ $cm^{-3}$. For a further increase of the laser power (~14 W), a reduction of the surface concentration ($5\times10^{18}$ $cm^{-3}$) was observed while the depth increased (4 µm) [12]. Thus, for the investigated *fPassDop* process, a compromise between surface concentration and profile depth is necessary.

Table 1 shows the IV results for the respective *PassDop* solar cells. The solar cells with PVD contacts—which received only a dummy firing—showed that the firing stable $SiN_x$ based *PassDop* worked well at the device level. The high open-circuit voltages $V_{oc}$ > 670 mV proved a good passivation for both the single layer as well as the *fPassDop* Gen 1. As they featured the same front side, the short-circuit current density $J_{sc}$ around 39 mA/$cm^2$ was the same for both approaches. A strong difference however can be observed concerning the fill factor *FF*. With 77.7 %, the *FF* for the single layer was found to be considerably lower compared to *fPassDop* Gen1 (80.1 %). Based on the high pseudo fill factor *PFF* for both layers, the loss in *FF* can be attributed to a higher series resistance of the single layer *PassDop* cell [13]. This high series resistance is a consequence of the low surface concentration in the doping profile for the single layer, which was determined to be in the range of 2-4×$10^{18}$ $cm^{-3}$, while for *fPassDop* Gen 1 a surface concentration of $1\times10^{19}$ $cm^{-3}$ was determined. The low surface concentration for the single layer results in a contact which is not fully ohmic. In total, the *fPassDop* process showed a much better and more reliable performance, with an average efficiency of 20.7 % compared to 19.6 % for the single layer. Thus for further development we focused on the *fPassDop* system.

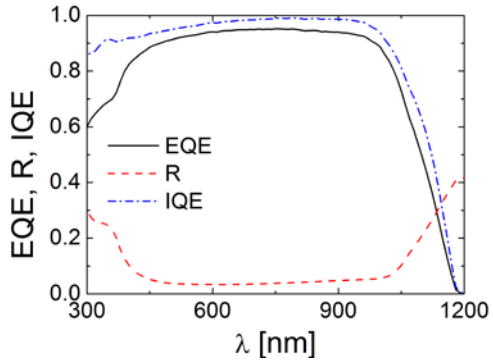


Figure 8: External and internal quantum efficiency and reflection for the screen printed *fPassDop* cell. The reflection curve was measured without bus bar.

As the results with PVD front contacts show a successful transfer to the device level, we fabricated large area (125×125 mm$^2$) solar cells with screen printed, to prove the compatibility with screen printing. These cells were processed with the improved *fPassDop* Gen 2 layer. The results for the best cell of this batch are shown in Table 1. This cell featured a high $V_{oc}$ of 668 mV, a $J_{sc}$ of 38.4 mA/cm² and a  of 78.2 %. This resulted in an energy conversion efficiency of 20.1 %. Particularly the high $V_{oc}$ of the screen printed solar cells close to 670 mV show the effective passivation of this solar cell. However, the measured IQE showed a significantly decreased efficiency in the short wavelength range of 300 nm to 700 nm (Figure 8), showing the recombination due to the screen printed contacts. $J_{sc}$ was mainly influenced by the metal-fraction and hence the shading (approx. 7 %) of the cell, which resulted in a loss of around 2.2 mA/cm$^2$. An optimized grid should improve $J_{sc}$ considerably. To characterize the loss due to internal reflection, we processed *fPassDop* cells with a $MgF_2$ reflector on the rear side. A comparison of the external quantum efficiencies (see Figure 9) of cells with and without the additional $MgF_2$ layer shows that by improving the reflection on the rear side, up to 0.53 mA/cm$^2$ can be gained in $J_{sc}$. The main influence due to the screen printed contacts for this cell was found in the fill factor of 78.2 %. This was mainly a result of the difference between the fill factor and the pseudo fill factor (SP: -4.7 %; PVD: -2.8 %), which is proportional to the series resistance [13]. Since the rear side of the cells (compared to *fPassDop* Gen 1) was similar or better regarding the

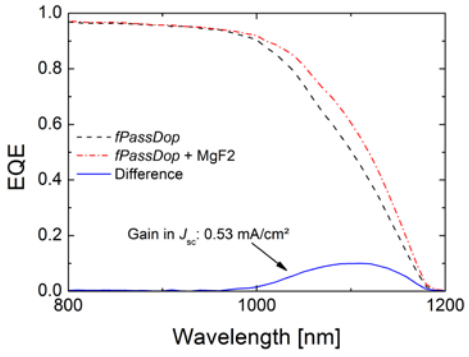


Figure 9: Comparison of the external quantum efficiency for screen printed *fPassDop* cells with and without a $MgF_2$ rear side reflector.

doping concentration, this difference in the series resistance most probably can be attributed to the front side screen printing.

## 4 CONCLUSION

In this work, we introduced a new, firing stable *PassDop* process (*fPassDop)* based on firing-stable a-$SiN_x$:P. This layer provides an effective surface passivation resulting in effective surface recombination velocities below 5 cm/s after a high temperature process as used for firing of screen printed contacts. The layer contains a sufficient amount of dopants to create a LBSF with a sheet resistance in the range of 60 Ω/sq and a surface concentration of about 1x10$^{19}$ cm$^{-3}$ after the laser process. This process was successfully transferred to the device level, reaching a conversion efficiency of 21.3 % (675 mV) in a first batch with small area solar cells (20×20 mm²) with PVD front side contacts. For large area solar cells (125×125 mm$^2$) with screen printed contacts efficiencies up to 20.1 % were reached with a voltage of up to 668 mV. These first results already show the high potential of the *fPassDop* process and indicate ways for further improvement.

## ACKNOWLEDGEMENTS

The authors would like to thank P. Hartmann, N. Hoffmann, N. König, V. Krumm, A. Leimenstoll, F. Schätzle, S. Seitz, A. Tuschinsky, N. Weber and K. Zimmermann for the processing of the solar cells and E. Schäffer and T. Hultzsch for measurements.

## REFERENCES

[1] J. Benick, B. Hoex, M.C.M. van de Sanden, W.M.M. Kessels, O. Schultz, S.W. Glunz High efficiency n-type Si solar cells on $Al_2O_3$-passivated boron emitters, Appl. Phys. Lett., 92 (2008) 253504/253501-253503.

[2] D. Suwito, U. Jäger, J. Benick, S. Janz, M. Hermle, S.W. Glunz Industrially feasible rear passivation and contacting scheme for high-efficiency n-type solar cells yielding a $V_{oc}$ of 700 mV, IEEE Trans. Electron Devices, 57 (2010) 2032-2036.

[3] S. Gatz, T. Dullweber, V. Mertens, F. Einsele, R. Brendel, Firing stability of $SiN_y$/$SiN_x$ stacks for the surface passivation of crystalline silicon solar cells, Sol. Ener. Mater. Sol. Cells, 96 (2012) 180-185.

[4] A.G. Aberle, Overview on SiN surface passivation of crystalline silicon solar cells, Sol. Ener. Mater. Sol. Cells, 65 (2001) 239-248.

[5] M. Kunst, O. Abdallah, F. Wünsch, Passivation of silicon by silicon nitride films, Sol. Ener. Mater. Sol. Cells, 72 (2002) 335-341.

[6] S. Dauwe, L. Mittelstädt, A. Metz, R. Hezel, Experimental evidence of parasitic shunting in silicon nitride rear surface passivated solar cells, Progr. Photovolt., 10 (2002) 271-278.

[7] S. Wenham, M. Green, Self Aligning Method For Forming a Selective Emitter and Metallization in a Solar Cell, in: United States Patent Application Publication, United States, 2002.

[8] B. Paviet-Salomon, S. Gall, R. Monna, S. Manuel, A. Slaoui, L. Vandroux, R. Hida, S. Dechenaux, Laser

doping using phosphorus-doped silicon nitrides, Energy Procedia, 8 (2011) 700-705.
[9] B. Paviet-Salomon, S. Gall, A. Slaoui, Investigation of charges carrier density in phosphorus and boron doped SiNx:H layers for crystalline silicon solar cells, Mater. Sci. Eng. B, 178 (2013) 580-585.
[10] A.B. Sproul, Dimensionless solution of the equation describing the effect of surface recombination on carrier decay in semiconductors, J. Appl. Phys., 76 (1994) 2851-2854.
[11] M.J. Kerr, A. Cuevas, General parameterization of Auger recombination in crystalline silicon, J. Appl. Phys., 91 (2002) 2473-2480.
[12] U. Jäger, D. Suwito, J. Benick, S. Janz, R. Preu, A laser based process for the formation of a local back surface field for n-type silicon solar cells, Thin Solid Films, 519 (2011) 3827-3830.
[13] J. Greulich, M. Glatthaar, S. Rein, Fill factor analysis of solar cells' current–voltage curves, Progr. Photovolt., 18 (2010) 511-515.